JOURNAL

OF THE AMERICAN CHEMICAL SOCIETY

VOLUME 110, NUMBER 15 JULY 20, 1988

Fluoride Affinities of Perfluorobenzenes C_6F_5X. Meisenheimer Complexes in the Gas Phase and Solution

Glen W. Dillow and Paul Kebarle*

Contribution from the Chemistry Department, University of Alberta, Edmonton, Canada T6G 2G2. *Received January 7, 1988*

Abstract: Measurements of gas-phase fluoride transfer equilibria lead to $\Delta G°$ and $\Delta H°$ for the reaction

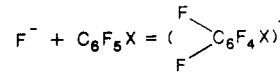

where the substituents X of the perfluorobenzenes are F, H, CF_3, $COCH_3$, CN, and NO_2. The relative energy changes are found to lead to an approximately linear correlation with the electron affinities of C_6F_5X. The gas-phase $\Delta G°$ and $\Delta H°$ data are used in combination with rate measurements in solution from the literature for a comparison of the reaction coordinates in the gas phase and solution and for determinations of the solvation energy of the transition state occurring in solution.

Anionic complexes that form as stable or transient species from the covalent addition of nucleophiles to substituted aromatic or heteroaromatic compounds have been subjects of interest and study since their discovery by Jackson[1] and Meisenheimer.[2] The "Meisenheimer complexes" are of particular significance since many aromatic nucleophilic substitutions S_NAr most likely proceed via such intermediates,[3] see eq 1.

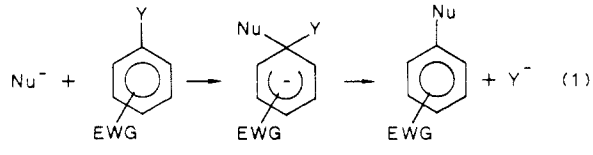

(1)

Studies of the relative stabilities of Meisenheimer complexes (ethoxide anion adducts to trinitrobenzene derivatives in methanol) were initiated by Caldin et al.[4] and followed by numerous systematic studies that have been reviewed recently by Terrier.[5]

Recent studies of gas-phase aliphatic S_N2 ion–molecule reactions[6-7] as for example reaction 2 did provide the the energy of

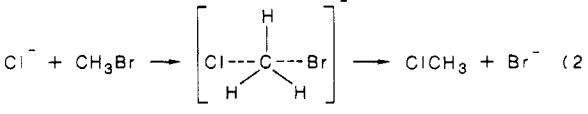

(2)

the transition state relative to the reactants and also the energies of species at other critical points of the gas-phase reaction coordinate. Comparison of the reaction coordinate in the gas phase with that in solution allowed one to evaluate the solvent effects on the reactants and the transition state. The experimental gas-phase ion–molecule work did also stimulate ab initio calculations of the structure and energy of the gas-phase transition states[9] as well as Monte Carlo simulations of S_N2 reactions in solution providing the reaction coordinate in solution and very interesting insights into the effects of protic and dipolar aprotic solvents.[9]

The present work which presents gas-phase ion–molecule reaction measurements aims to provide similar gas-phase information and comparisons with experimental results in solution but now for aromatic S_N2 type reactions proceeding via Meisenheimer complexes. In this paper, we describe results for the complexes of substituted perfluorobenzenes with F^-. Work involving substituted nitrobenzenes and methoxy anions is in progress and will be reported on in the near future.[10]

Experimental Section

The F^- transfer equilibria measurements were performed with a pulsed high-pressure mass spectrometer, PHPMS, that has been described.[11]

(1) Jackson, C. J.; Gazzolo, F. H. *Am. Chem. J.* **1900**, *23*, 376.
(2) Meisenheimer, J. *Justus Liebigs Ann. Chem.* **1902**, *323*, 205.
(3) Bunnett, J. F.; Zahler, R. E. *Chem. Rev.* **1951**, *49*, 273. Miller, J. *Aromatic Nucleophilic Substitution*; Elsevier: Amsterdam, 1968.
(4) Caldin, E. F.; Long, G. *Proc. R. Soc. London, Ser. A* **1955**, *226*, 263. Ainscough, J. B.; Caldin, E. F. *J. Chem. Soc.* **1956**, 2540.
(5) Terrier, F. *Chem. Rev.* **1982**, *82*, 77.
(6) (a) Farneth, W. E.; Brauman, J. I. *J. Am. Chem. Soc.* **1976**, *98*, 7891. (b) Olmstead, W. N.; Brauman, J. I. *J. Am. Chem. Soc.* **1977**, *99*, 4219. (c) Asubiojo, O. I.; Brauman, J. I. *Ibid.* **1979**, *101*, 3715.
(7) Caldwell, G.; Magnera, T. F.; Kebarle, P. *J. Am. Chem. Soc.* **1984**, *106*, 959.
(8) Magnera, T. F.; Caldwell, G.; Sunner, J.; Ikuta, S.; Kebarle, P. *J. Am. Chem. Soc.* **1984**, *106*, 6140. Kebarle, P.; Caldwell, G.; Magnera, T.; Sunner, J. *Pure Appl. Chem.* **1985**, *57*, 339.
(9) Chandrasekhar, J.; Smith, S. F.; Jorgensen, W. L. *J. Am. Chem. Soc.* **1984**, *106*, 3049. Chandrasekhar, J.; Jorgensen, W. L. *Ibid.* **1985**, *107*, 2974 and references therein.
(10) Paul, J. G. C.; Kebarle, P., in preparation.
(11) Kebarle, P. In *Techniques of Chemistry*; Saunders, W. H., Farrar, J. M., Eds.; Wiley Interscience: New York, 1988.

0002-7863/88/1510-4877$01.50/0

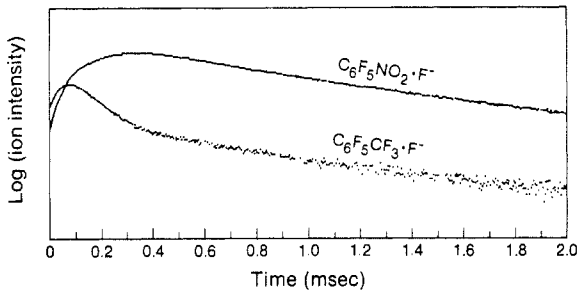

Figure 1. Time dependence of ion intensities of F^- adducts to $C_6F_5NO_2$ and $C_6F_5CF_3$. A logarithmic scale is used for intensities. Ion source temperature 150 °C, 0.68 mTorr of $C_6F_5NO_2$, 68.1 mTorr of $C_6F_5CF_3$, 240 mTorr of NF_3. Bath gas CH_4, total pressure 4 Torr. F^- produced by dissociative electron capture by NF_3 is rapidly captured by $C_6F_5CF_3$. Fluoride transfer to the higher fluoride affinity $C_6F_5NO_2$ leads to achievement of equilibrium after ~0.5 ms.

The experimental procedure was similar to that used for the determinations of electron-transfer equilibria.[12]

A representative result is shown in Figure 1. An electron pulse of ~10 μs produces secondary near-thermal electrons. NF_3 is used for the production of F^- by the electron capture: $NF_3 + e = F^- + NF_2$. For the conditions used, F^- adds on rapidly to the perfluorobenzenes and disappears very early. Therefore its concentration is not shown. In addition to the fluoride adducts shown, also the electron adducts, i.e., the radical anions $C_6F_5NO_2^{\bullet-}$ and $C_6F_5CF_3^{\bullet-}$, were observed. Since the electron capture coefficients of the perfluorobenzenes are relatively large, while NF_3 has a small coefficient for capture of thermal electrons, a high pressure of NF_3 had to be used to enhance the production of F^- relative to that of the radical anions.

The NF_3 gas obtained from Ozark-Mahoning, Tulsa, Oklahoma, contained some HF. This had to be removed in order to prevent the fluoride transfer reaction: $C_6F_6X^- + HF = FHF^- + C_6F_5X$. Since part of the gas handling plant is out of glass, the presence of HF also led to production of BF_3, SiF_4, and other fluorinated silanes which interfered with the measurements due to their very high fluoride affinities. Most of the HF could be removed by passing slowly the NF_3 gas at 1 atm through a $^1/_4$ in. i.d. stainless steel U tube immersed in an ethanol slush bath (−117 °C).

Results and Discussion

(a) Gas-Phase Fluoride Affinities. The gas-phase ion–molecule equilibria, of 3, involving F^- transfer were measured with a pulsed electron high ion source pressure mass spectrometer PHPMS.[11] The establishment of a typical equilibrium is illustrated in Figure

$$F^-C_6F_5X + C_6F_5Y = C_6F_5X + F^-C_6F_5Y \quad (3)$$

$$K_3 = \frac{[F^-\cdot C_6F_5Y]}{[F^-\cdot C_6F_5X]}\frac{[C_6F_5X]}{[C_6F_5Y]} \quad (4)$$

$$-\Delta G^\circ_3 = RT \ln K_3 \quad (5)$$

1. A short, tens of μs, electron pulse creates near-thermal electrons. Dissociative electron capture by the NF_3 leads to F^-, see Experimental Section, which rapidly adds to the two perfluorobenzenes. Since the (trifluoromethyl)benzene is present at a much higher concentration, the formation of its fluoride is more rapid, see first 50 μs in Figure 1. Fluoride transfer 3 leads to formation of the more stable nitrobenzene fluoride. Equilibrium 3 is achieved at the point where the vertical distance between the two ion intensities becomes constant since this corresponds to a constant ion ratio in the logarithmic plot used. The equilibrium constants K_3 were obtained by substituting the detected ion intensities at equilibrium and the known concentrations of the two neutral perfluorobenzenes. The equilibrium constant $K_3 = 7620$ results from the data in Figure 1. Free energy changes ΔG°_3 are evaluated via eq 5.

The ΔG°_3 values for the interconnected exchange reactions that were studied are shown in Figure 2. These values can be combined to obtain the ΔG°_{FT}, the fluoride transfer free energy relative to C_6F_6, see eq 6, and these data are shown in Figure 2 and Table I.

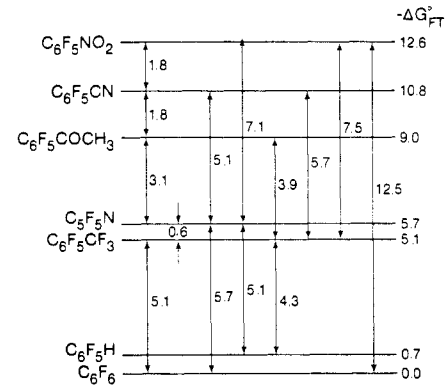

Figure 2. ΔG°_3 results for F^- transfer reaction 3 at 150 °C in kcal·mol^{-1} beside arrows. ΔG°_{FT} corresponds to free energy for fluoride transfer from C_6F_6 to the respective compound at 150 °C. ΔG°_{FA} is the free energy for reaction 7, and ΔH°_{FA} (fluoride affinity) is the corresponding enthalpy change. The ΔG°_{FT} and ΔH°_{FT} = −22.7 kcal·mol^{-1} and ΔS°_{FT} = −23.7 cal·K^{-1}·mol^{-1} for C_6F_6 obtained by Hiraoka.[13] All energies are in kcal·mol^{-1}.

Table I. Thermochemical Data Leading to ΔG° and ΔH° for the Reaction $F^- + C_6F_5X = C_6F_6X^-$

compound B	$(\sigma_B/\sigma_{BF^-})^a$	$(-\Delta G^\circ_{FT})^b$	$(-\Delta H^\circ_{FT})^c$	$(-\Delta G^\circ_{FA})^d$	$(-\Delta H^\circ_{FA})^e$
C_6F_6	6	0	0	20.0[f]	27.0[f]
C_6F_5H	1	0.7	2.2	20.7	29.2
$C_6F_5CF_3$	1	5.1	6.6	25.1	33.6
$C_6F_5COCH_3$	1	9.0	10.5	29.0	37.5
C_6F_5CN	1	10.8	12.3	30.8	39.3
$C_6F_5NO_2$	1	12.6	14.1	32.8	41.1

[a] Ratio of rotational symmetry numbers used to evaluate ΔS°_{FT}. [b] Free energy change for fluoride transfer from C_6F_6 to C_6F_5X, see eq 6, at 150 °C, from Figure 2, in kcal·mol^{-1}. [c] Enthalpy for fluoride transfer eq 6 in kcal·mol^{-1}. [d] Free energy fluoride affinity, see eq 7 in kcal·mol^{-1}. [e] Fluoride affinity, see eq 7 in kcal·mol^{-1}. [f] Data due to Hiraoka.[13]

$$C_6F_7^- + C_6F_5X = C_6F_6 + C_6F_6X^- \quad (6)$$

$$\Delta G^\circ_6 = \Delta G^\circ_{FT}$$

Generally the entropy changes for exchange reactions like (3) and (6) are quite small, such that $T\Delta S$ is less than 1 kcal·mol^{-1}.[12] Since the temperature dependence of reactions 3 and thus also 6 was not determined, ΔS°_6 was estimated by considering the rotational symmetry numbers σ only and ΔS°_6 was assumed to be equal to the entropy change due rotational symmetry only:

$$\Delta S^\circ_6 \approx R \ln (\sigma_A\sigma_B/\sigma_C\sigma_D)$$

$$\Delta S^\circ_6 \approx -3.56 \text{ cal·K}^{-1}\text{·mol}^{-1}$$

where A and B are the reactants and C and D the products. The σ values used are shown in Table I. Due to cancellations, ΔS°_6 is constant for reactions 6 and equal to −3.56 cal·K^{-1}·mol^{-1}. The ΔH°_6 values evaluated with this assumption are given in Table I. The absolute fluoride affinities ΔH°_7 and free energies ΔG°_7 can then be obtained by calibrating to the known values for C_6F_6.

$$C_6F_6 + F^- = C_6F_7^- \quad (7)$$

$$\Delta H^\circ_7 = -27 \text{ kcal·mol}^{-1}\ [13]$$

$$\Delta S^\circ_7 = -23.5 \text{ cal·deg}^{-1}\text{·mol}^{-1}\ [13]$$

$$C_6F_5X + F^- = C_6F_6X^-$$

The ΔH°_7 and ΔS°_7 for C_6F_6 were obtained recently by Hiraoka et al.,[13] who determined the temperature dependence of the equilibria with a PHPMS. These authors also performed ab initio calculations which provided theoretical results for ΔH°_7 and ΔS°_7 for C_6F_6 which were in very good agreement with the experimental results. The theoretically obtained structure of $C_6F_7^-$ showed that

(12) Kebarle, P.; Chowdhury, S. *Chem. Rev.* **1987**, *87*, 513.

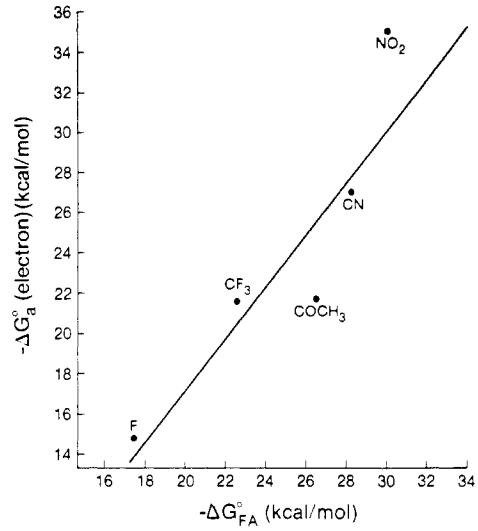

Figure 3. Fluoride attachment energies, $\Delta G°_7$, from Table I, versus electron attachment energies $\Delta G°_a$, from Kebarle,[12] for compounds C_6F_5X. Slope of line 1.36, correlation coefficient 0.909.

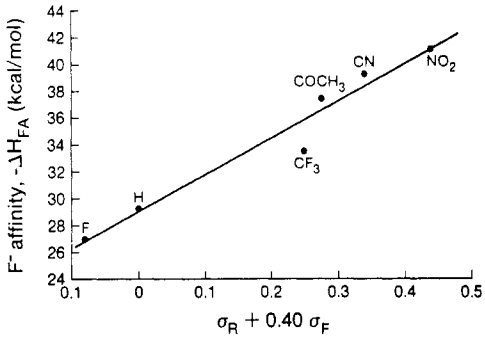

Figure 4. Fluoride affinities $\Delta H°_7$ for C_6F_5X from Table I versus substituent parameters for the para position of Taft,[14] see fluoride structure I. Slope ρ = 27.8; correlation r : 0.979.

there are two equidistant fluorine atoms associated with the same carbon atom which means that the $C_7F_7^-$ obtained from the gas-phase reaction 7 has the expected Meisenheimer complex structure.

The fluoride affinities, $\Delta H°_7$ and $\Delta G°_7$, for the substituted perfluorobenzenes obtained by combining the present $\Delta H°_6$ with Hiraoka's data are also given in Table I.

A plot of the electron attachment free energies[12] of the C_6F_5X compounds $\Delta G°_a$ versus the F^- attachment energies, $\Delta G°_7$, is shown in Figure 3. A fairly good linear relationship (linear regression coefficient r = 0.909) with a slope of 1.4 is observed. The relationship is not unexpected. The energy of the π*LUMO of the substituted fluorobenzene which accepts the electron that leads to the radical anion is decreased by the presence of electron-withdrawing substitutents X. On formation of the fluoride, the π* mixed with the lowest σ* makes a contribution to the stability of the $C_6F_6X^-$ Meisenheimer complex.[13]

A plot of the fluoride affinities $\Delta H°_7$ versus the Taft[14] σ_R and σ_F substituent parameters is shown in Figure 4. A good linear relationship is observed (correlation coefficient r = 0.979), slope ρ = 27.8. The factor 0.4 with which the field effect substituent constant σ_F is multiplied has the value that leads to the best correlation. It is interesting to note that exactly the same factors for σ_R and σ_F lead to the best correlation of the electron acceptor substituent constants with the gas-phase acidities of the phenols (r = 0.998).[14]

Analysis of products from aromatic nucleophilic substitutions of perfluorophenyls indicates[15] that the nucleophile, F^-, inserts

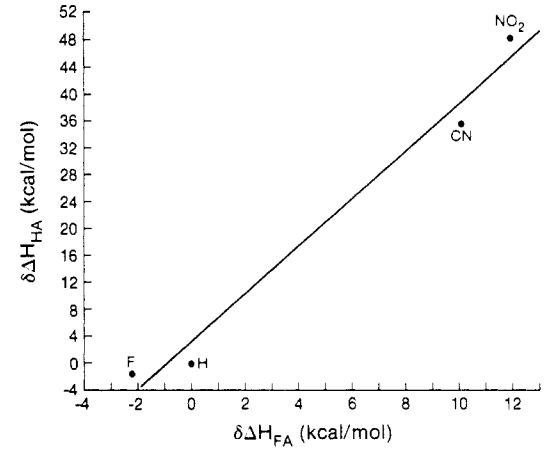

Figure 5. Hydride affinities of C_6H_5X calculated by Radom[16] versus fluoride affinities of C_6F_5X from table I. Slope = 3.5; correlation coefficient r = 0.990.

preferentially in the 4 position relative to the electron-withdrawing substituent. Therefore, we assume that the perfluoro Meisenheimer complexes whose energies are given in Figures 1–4 and Table I are 1,4 complexes as shown in structure I. This assumption is also in line with the use of the substituent constants for the para position in Figure 4.

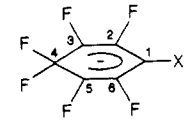

I

Radom et al.[16] have reported ab initio calculations with the minimal STO-3G basis set of the hydride adducts to substituted benzene shown in structure II.

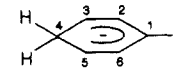

II

A plot of the relative hydride affinities obtained by Radom[16] versus the fluoride affinities from the present work is shown in Figure 5. The straight line has a correlation coefficiencies r = 0.990 and a slope of 3.5.

Radom's[16] calculations predict that for X = F, the hydride affinity of C_6H_5X is increased significantly when F is in positions 2 or 6 (meta), 6.7 kcal·mol^{-1}, and 4 (ipso), 6.9 kcal·mol^{-1}, slightly in positions 3 and 5 (ortho), 2.4 kcal·mol^{-1}, and is decreased by 1.7 kcal·mol^{-1} for position 1 (para), see structure II. These results are consistent with the expected destabilization by F due to π donation in the ortho and para positions and the strong stabilization due to the field effect which is weakest for the para position.

The above results support the assumed structure III for the fluoride adduct to C_6F_5H. In III the destabilizing effect of F in

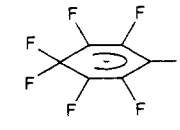

III

the para position is avoided while stabilization by F is obtained in the other positions and particularly the ipso and meta positions. On this basis, the higher fluoride affinity for C_6F_5H relative to C_6F_6, observed experimentally, see Figure 2 and Table I, is expected.

The very large slope, ρ = 3.5, in Figure 5, assuming that the calculations are approximately correct, which is generally the case

(13) Hiraoka, K.; Mizuse, S.; Yamabe, S. *J. Chem. Phys.* **1987**, *86*, 4102.
(14) Fujio, M.; McIver, R. T.; Taft, R. W. *J. Am. Chem. Soc.* **1981**, *103*, 4017. Taft, R. W.; Topsom, R. D. *Prog. Phys. Org. Chem.*, in press.
(15) Ho, K. C.; Miller, J. *Aust. J. Chem.* **1966**, *19*, 423.
(16) Birch, A. J.; Hinde, A. L.; Radom, L. *J. Am. Chem. Soc.* **1980**, *102*, 6430.

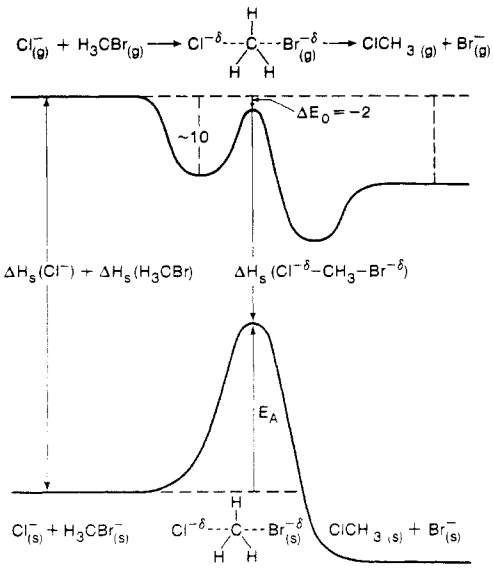

Figure 6. Comparison of the reaction coordinate for an aliphatic S_N2 reaction in the gas phase and solution. From Magnera.[8]

for isodesmic reaction energy changes,[16] should be due to two factors. First, due to stabilization by the five F atoms, see structure I, the demand on the electron-withdrawing substituent X will be much smaller than in the nonperfluorinated adduct, see II. Second, due to the smallness of H^- relative to F^-, a larger stabilization due to the attendant expansion of the charge is expected when H^- rather than F^- adds to a given benzene. This means that the stabilizing effect of the substituent will be more important and thus larger for H^- rather than F^-.

(b) Reaction Coordinates of Aromatic Substitution Reactions in the Gas Phase and in Solution. Solvation Energy of the Transition State. As mentioned in the introduction, comparisons of the reaction coordinates of aliphatic S_N2 reactions in the gas phase and solution[6-7] provide valuable insights. As an example we reproduce in Figure 6 the reaction coordinates for reaction 2. The reaction coordinate expected in the gas phase for the aromatic S_N2 reaction 7 where X = F and the corresponding reaction in DMSO solution are shown in Figure 7. The activation energy in solution is from the study of the F^{18} exchange in DMSO, by Cacace and co-workers.[17]

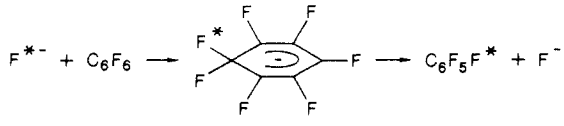

There is an important difference between the gas-phase reaction coordinates in Figures 6 and 7. For the aliphatic substitution, the transition state in the gas phase lies on a local energy maximum and this state and the transition state in solution probably have very similar geometries. For the aromatic substitution, Figure 7, the bottleneck of the gas-phase kinetics, i.e., the gas-phase transition state, occurs at the centrifugal barrier, which is not shown in Figure 7, but its position is indicated by an arrow. This transition state has nothing to do with the transition state in solution; however, the potential energy change in the gas phase is of importance to the process in solution, vide infra.

The details of the gas-phase potential energy change, Figure 7, are not known. The depth of the well where the $C_6F_7^-$ is "located" used in Figure 7 is due to Hiraoka's results. The two symmetric wells, indicated with a depth of ~5 kcal·mol^{-1}, indicate the intermolecular bonding $F^-\cdots C_6F_6$ complexes. C_6F_6 has a quadrupole moment of a sign opposite to that for C_6H_6,[13] i.e., the approach of F^- along the C_6 symmetry axis is attractive for C_6F_6 and so an intermolecular bond energy of ~5 kcal·mol^{-1} can be

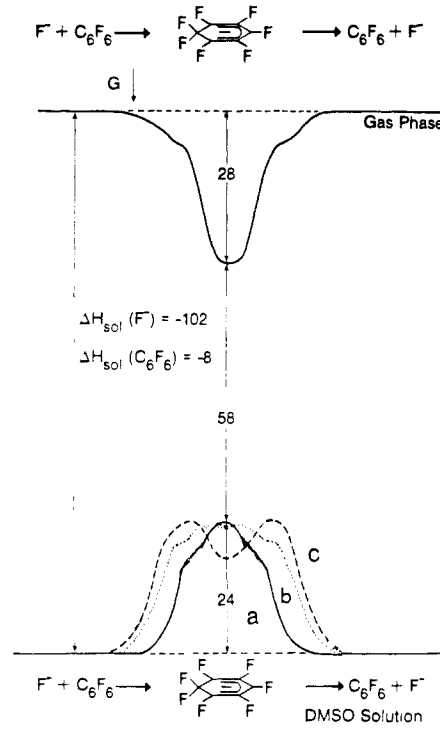

Figure 7. Reaction coordinates for the aromatic S_N2 reaction in the gas phase and in DMSO solution. The arrow marked G indicates the probable location of the gas-phase transition state due to the centrifugal barrier. Activation energy of 24 kcal·mol^{-1} in DMSO due to Cacace.[17] Potential energy curves a, b, and c illustrate three possible consequences of the decrease of the solvation energy. In (c) the early humps due to displacement of one DMSO molecule by C_6F_6 from the inner solvation shell of F^- dominate. In (b) and (a) the early desolvation is assumed to be progressively less important. Shapes like (b) or (a) are believed to be indicated by the data. Due to the higher fluoride affinity of $C_6F_5NO_2$ a shape like c is believed to occur for the reaction $F^- + C_6F_5NO_2$ in solution.

expected for this complex. There can be little doubt that the approach of F^- to C_6F_6 in the gas phase is attractive all the way to the formation of $C_6F_7^-$. Yamabe[18] has reported results from theoretical calculations (MNDO and 4-31G + P) predicting the potential energy change for reaction 8, which show a continuous

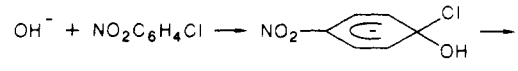

$$NO_2C_6H_4OH + Cl^- \quad (8)$$

decrease of energy on formation of the Meisenheimer complex. These results are in support of the assumed gas-phase potential energy in Figure 7; however, the analogy is not very close since the potential energy of (8) is strongly affected by the large exothermicity for this reaction.

The solvation energy of F^- in DMSO, $\Delta H_{sol}(F^-) = -102$ kcal·mol^{-1}, shown in Figure 7 was estimated as shown in the Appendix. The precision of the value is unknown but an uncertainty of ±5 kcal·mol^{-1} or more is to be expected. The origin of the data for $\Delta H_{sol}(C_6F_6) = -8$ kcal/mol^{-1} is also given in the Appendix.

Since the solvation energy of F^- is so big one could expect that the initial increase of the energy as C_6F_6 and F^- approach each other will be almost entirely due to desolvation of F^-. Thus, a significant increase of energy should occur as C_6F_6 slips into a position in the inner solvation shell of F^-, displacing in the process a DMSO molecule. The distance between C_6F_6 in the inner shell and F^- may be large enough so that only a small fraction of the stabilization due to the covalent interaction ultimately leading to the Meisenheimer complex is present. The energy increase due to such an F^- desolvation step could be as large as 20 kcal·mol^{-1},

(17) Cacace, F.; Speranza, M.; Wolf, A. P.; MacGregor, R. R. *J. Fluorine Chem.* **1982**, *21*, 145.

(18) Yamabe, S.; Minato, T.; Kawabata, Y. *Can. J. Chem.* **1984**, *62*, 235.

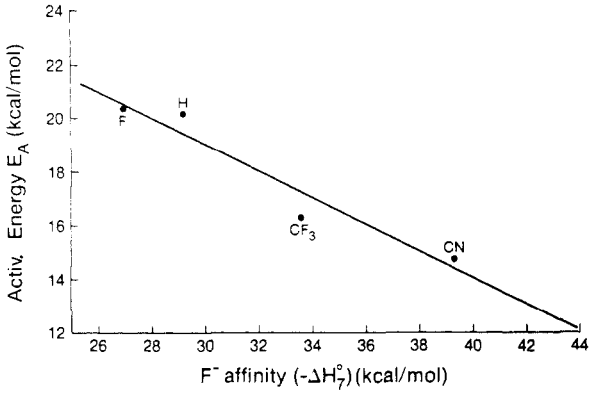

Figure 8. Plot of activation energies for reaction $CH_3O^- + C_6F_5X \rightarrow CH_3OC_6F_5X^- \rightarrow CH_3OC_6F_4X + F^-$ in methanol from Ho and Miller[15] versus fluoride affinities of C_6F_5X from Table I.

see Appendix. As the C_6F_6 moves even closer to the F^-, a large release of energy due to covalent bonding will occur. However, since the covalent bond formation causes a simultaneous negative charge expansion from F^- to the very delocalized charge distribution in $C_6F_7^-$, the solvation energy of the negative ion complex decreases greatly. The net effect may lead to energy changes as in curves a–c in Figure 7.

Assuming that the potential energy is similar to curve a or b, the solvation energy of the Meisenheimer complex $C_6F_7^-$ will be given by the vertical line in Figure 6 which leads to the values shown in eq 9

$$\Delta H^\circ_{sol}(C_6F_7^-) \approx -58 \text{ kcal·mol}^{-1} \text{ (in DMSO)} \qquad (9)$$

for

$$\Delta H^\circ_{sol}(F^-) \approx -102 \text{ kcal·mol}^{-1} \text{ (in DMSO)}$$

The $C_6F_7^-$ solvation value can be compared with results for the solvation of the $C_6F_6^{\bullet-}$ radical anion obtained from polarographic half-wave potential measurements of the reduction of C_6F_6. As shown in the Appendix, $\Delta H^\circ_{sol}(C_6F_6^{\bullet-}) \approx -54$ kcal·mol^{-1} in DMF can be estimated from these results. The solvation energy in DMSO, considering that the charge is highly delocalized, should be close to that in DMF. One may expect that $C_6F_6^{\bullet-}$ should have a solvation energy that is close to that of $C_6F_7^-$. A net atomic charge distribution in $C_6F_7^-$ is given in Hiraoka.[13] A large fraction of the charge is quite evenly distributed over the seven fluorines while the rest is in the (π system) carbon atoms. For $C_6F_6^{\bullet-}$ one may expect a similar charge distribution considering that the fluorines are essential to the stabilization of the negative ion.[12,19]

Thus, $\Delta H_{sol}(C_6F_7^-) \approx \Delta H_{sol}(C_6F_6^{\bullet-}) \approx -54$ kcal·mol^{-1} is a reasonable choice and this value is close to the solvation energy of -58 kcal·mol^{-1}, see eq 9, deduced from the Born cycle in Figure 6 and curve a or b. While the estimate is not accurate enough to eliminate curve c it suggests that the central well depth of curve c cannot be more than a few kcal·mol^{-1} deep.

The fluoride affinities for the C_6F_5X given in Table I can be used to extend the comparison of the gas-phase and solution data over this series. Unfortunately, solution activation energies for reaction 7 where F^- is the nucleophile and C_6F_5X the electron donors are not available. The closest data[17] are those for CH_3O^- as nucleophile, see eq 10, in methanol. A plot of the activation

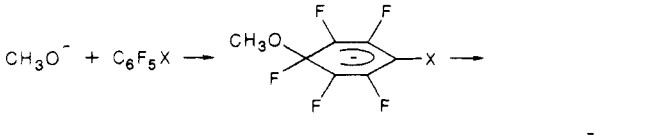

$$1,4\text{-}CH_3OC_6F_4X + F^- \qquad (10)$$

energies E_A in methanol versus the fluoride affinities from Table I is shown in Figure 8. The approximate linear relationship (r = 0.96) has a slope $\rho = -0.5$, i.e., the activation energy in solution decreases as the bond energy in the complex, i.e., the fluoride affinity, increases.

The activation energy for reaction 10 for perfluorobenzene in methanol is 20.4 kcal·mol^{-1},[16] see Figure 7, which is lower than the 24 kcal·mol^{-1} activation energy for reaction 8 where F^- is the nucleophile and DMSO the solvent. This difference probably reflects the somewhat lower solvation energy of CH_3O^- relative to F^-, a difference that is partially offset by the stronger solvating ability of the protic methanol toward small ions when compared to DMSO.

In the absence of a substituent effect on the solvation of the Meisenheimer complex $CH_3OC_6F_5X^-$ and for potential energy curves such as a in Figure 7 the slope in Figure 8 should have been close to unity. The $\rho = -0.5$ is due either to a substituent effect on the solvation of the complex and curves such as a or to substituent effect on solvation and curves such as c. It is clear, that the farther the maxima in curves of type c are displaced from the center, the smaller will be the contribution of the covalent bonding of the gas-phase complex to the activation energy and thus the smaller will be the value of $-\rho$.

The substituent effect on the solvation of the highly delocalized $XC_6F_5CH_3O^-$ complexes can be expected to be quite small, see for example Figure 17 in Taft[20] giving acidities of carbon acids in the gas phase and DMSO, which has a slope close to unity. A similar result is indicated also for solvents like methanol.[21] On this basis, the $\rho = -0.5$ observed in Figure 7 is likely not only due to a substituent effect on the solvation of the Meisenheimer complexes but also to an attenuation of the effect of the increasing gas-phase fluoride affinity by a gradual shift to reaction coordinates of the type c. Thus it is suggested that for X = F the coordinate is still type a or b but a shift to type c with a deepening well occurs as X becomes progressively more electron withdrawing.

Aromatic substitutions involving 1,3,5-tri-EWG-substituted benzenes, e.g., trinitrobenzene, which form stable Meisenheimer complexes with nucleophiles like CH_3O^- have been studied extensively in solution, see Table I in Terrier.[5] Typically, such complexes have potential energies as in type c, Figure 6, with a deep central well. On the basis of the present discussion, the activation energy for the formation of these complexes, i.e., the potential energy barrier to the left of the well, is not due to electronic factors, e.g., disturbed bonding in the intermediate, but largely due to the desolvation of the CH_3O^- nucleophile which occurs as the substituted benzene enters the inner solvation shell of the negative nucleophile.

The electron affinity of the trinitrobenzene is expected[12] to be very much larger than that of $C_6F_5NO_2$. Assuming that a relationship like that in Figure 3 can be extrapolated approximately to compounds with much higher EA like the trinitrobenzene, one can predict a much higher fluoride and a higher methoxide binding energy for this type of Meisenheimer complex. The observed[5] deep wells in the potential energies in solution are thus anticipated on the basis of the gas-phase data. As mentioned earlier, gas-phase measurements involving nitroaromatics and methoxyanions are presently underway in this laboratory[10] and should provide more direct data for comparison with the results in solution.[5]

Appendix: Thermochemical Data

(a) Solvation Energy of F^- and C_6F_6 in DMSO. The $\Delta H^\circ_{sol}(F^-)$ corresponding to the process $F^-_{(g)} \rightarrow F^-_{DMSO}$ was estimated by extrapolating the solvation energies of the halide ions in DMSO relative to that for Cl^-, see Figure 8 in Magnera,[8] to that for F^- at a radius of 1.33 Å. This extrapolation predicts that the solvation exothermicity of F^- is 22 kcal·mol^{-1} more exothermic than that for Cl^- in DMSO. This value together with the single ion hydration enthalpy $\Delta H_{sol}(Cl^-) = -81.3$ kcal·mol^{-1}, due to Randles and quoted by Desnoyer,[22] and the enthalpy of transfer of Cl^- from

(19) Chowdhury, S.; Grimsrud, E. P.; Heinis, T.; Kebarle, P. *J. Am. Chem. Soc.* **1986**, *108*, 3630.

(20) Taft, R. W. *Prog. Phys. Org. Chem.* **1983**, *14*, 247.

(21) Taft, R. W., private communication.

(22) Desnoyer, J. E. *Jolicoeur. Modern Aspects of Electron Chemistry*; Bockris, J. O. M., Conway, B. E., Eds.; Plenum: New York; Vol. 5. Reiss, J. R.; Heller, A. *J. Phys. Chem.* **1985**, *89*, 4207.

H_2O to DMSO $\Delta H°_{tr} \approx 1$ kcal·mol^{-1} (Parker[23]) leads to $\Delta H°_{sol}(F^-) \approx -102$ kcal·mol^{-1} in DMSO.

The $\Delta H_{sol}(C_6F_6) = -8$ kcal·mol^{-1} is based on the vaporization enthalpy of C_6F_6, $\Delta H°_{vap} = 8$ kcal·mol^{-1},[24] and the near-zero enthalpy of mixing of liquid C_6F_6 and DMSO.[25]

(b) Change of Solvation Energy of F^- in DMSO on Displacement of One Inner-Shell DMSO Molecule with C_6F_6. A rough value can be obtained by estimating first the solvation energy of $F^-(DMSO)_4$ in DMSO. The radius of $F^-(DMSO)_4$ was estimated as 5.5 Å (see Table IV in Magnera[8]). This radius then was used to obtain the solvation energy differences between Cl^- and $F^-(DMSO)_4$ in DMSO, via the same type of extrapolation in Figure 8 (Magnera[8]) as in part a. This difference was found to be 42 kcal·mol^{-1}. Since $\Delta H_{sol}(Cl^-) = -80.3$ kcal·mol^{-1} in DMSO, see part a, the $\Delta H_{sol}(F^-(DMSO)_4) \approx -38$ kcal·mol^{-1}. Since $-\Delta H_{sol}(F^-) = 102$ kcal·mol^{-1}, see part a, the contribution of the inner shell to the solvation can be taken as $102 - 38 = 54$ kcal·mol^{-1}, and replacing one of the DMSO molecules from the inner shell of F^- with the very inefficient C_6F_6 should lead to $^1/_4$ loss of inner-shell solvation, i.e., ~ 16 kcal·mol^{-1}. Considering that this is only a rough estimate, the actual energy increase due to desolvation could easily surpass 20 kcal·mol^{-1}.

(c) Solvation Energy of $C_6F_6^{\bullet-}$. The polarographic half-wave reduction potential of C_6F_6 in dimethylformamide (DMF) has been determined as $\epsilon_{1/2} = -2.1 \pm 0.1$ V versus the saturated calomel electrode (SCE). This value when substituted into eq 11, together with the known electron attachment free energy of

$$\Delta G°_{sol}(B^-) - \Delta G°_{sol}(B) = -108 \text{ (kcal·mol}^{-1}) - 23.06\epsilon_{1/2}(B) \text{ (V)} - \Delta G°_a(B) \quad (11)$$

$B = C_6F_6$, $\Delta G°_a(B) = -14.8$ kcal·mol^{-1},[12] leads to

$$\Delta\Delta G°(C_6F_6^{\bullet-}) = \Delta G°_{sol}(C_6F_6^{\bullet-}) - \Delta G°_{sol}(C_6F_6) = -45 \text{ kcal·mol}^{-1} \text{ in DMF} \quad (12)$$

For the origin of eq 11 see Heinis.[26] The numerical constant -108 kcal·mol^{-1} is based on the single ion hydration energy of Cl^- due to Randles and is thus consistent with the thermochemistry used in parts a and b of the Appendix.

The $\Delta\Delta G°(C_6F_6^{\bullet-}) = -45$ kcal·mol^{-1} is close to the corresponding values for 1,4-dinitrobenzene, $\Delta\Delta G° \approx -48$ kcal·mol^{-1},[27] and tetrafluorobenzoquinone, $\Delta\Delta G° \approx -48$ kcal·mol^{-1}.[26] These three radical anions are expected to be strongly charge delocalized. The available $\Delta\Delta S° = -5$ cal·K^{-1}·mol^{-1} (Parker[27]) for the dinitrobenzene is assumed to be valid also for C_6F_6. This assumption leads to $\Delta\Delta H°(C_6F_6^{\bullet-}) = -46.5$ kcal·mol^{-1} in DMF.

For strongly delocalized anions the values in DMF and DMSO should be close. Taking $\Delta H_{sol}(C_6F_6) = -8$ kcal·mol^{-1} in DMSO (see part a, Appendix), one obtains a rough estimate for $\Delta H_{sol}(C_6F_6^{\bullet-}) \approx -54.5$ kcal·mol^{-1} in DMSO.

Registry No. F, 16984-48-8; C_6F_6, 392-56-3; C_6HF_5, 363-72-4; $C_6F_5CF_3$, 434-64-0; $C_6F_5OCH_3$, 389-40-2; C_6F_5CN, 773-82-0; $C_6F_5NO_2$, 880-78-4; perfluorobenzene radical anion, 37551-90-9.

(23) Parker, V. B. *Thermal Properties of Aqueous Uni-univalent electrolytes*; National Bureau of Standards: Washington, D.C., 1965; NSRDS-NBS[2]. Wu, Y. C.; Friedman, H. L. *J. Phys. Chem.* **1966**, *70*, 501, 2020. Krishnan, C. V.; Friedman, H. L. *Ibid.* **1969**, *73*, 3934; **1970**, *74*, 2356; **1971**, *75*, 388 and 3606. Abraham, M. H. *J. Chem. Soc., Faraday Trans. I* **1973**, *69*, 1375.

(24) Cox, J. D.; Gundry, H. A.; Harrop, D.; Head, A. J. *J. Chem. Thermodyn.* **1969**, *1*, 77.

(25) Mattingley, B. I.; Handa, Y. P.; Fenby, D. V. *J. Chem. Thermodyn.* **1975**, *7*, 169.

(26) Heinis, T.; Chowdhury, S.; Scott, S. L.; Kebarle, P. *J. Am. Chem. Soc.*, in press.

(27) Svaan, M.; Parker, V. D. *Acta Chem. Scand.* **1982**, *B36*, 357.

Growth of Silver Halides from the Molecule to the Crystal. A Pulse Radiolysis Study

K. H. Schmidt, R. Patel,† and D. Meisel*

Contribution from the Chemistry Division, Argonne National Laboratory, Argonne, Illinois 60439. *Received January 14, 1988*

Abstract: Halide ions were produced in situ by pulse radiolysis, via electron transfer to dihalomethanes from solvated electrons or hydrogen atoms, and were then used to generate silver halide molecules and larger aggregates. This evolution of silver halide aggregates was studied for the case of silver iodide on the time scale of 10^{-6}–10^2 s. Conductivity detection allows determination of the rate of formation of the first AgI molecule. Spectrophotometric detection of the growth of the particles from the stage of the molecular species to colloidal particles of bulk electronic properties is then possible. When the aggregates thus formed approach sizes of ca. 50 Å, their detection by light scattering provides an independent method of size determination. In the region where such measurements are possible, the sizes determined by light scattering agree with sizes calculated assuming confinement of excitons in small particles and their electron-hole coulomb screening. A similar approach is suggested for growth studies of other insoluble materials.

The growth of silver halide particles has been a subject of many studies in conjunction with their application in photographic processes.[1] The growth mechanism is particularly important in such processes since the sensitivity of the photographic material depends on its grain size as well as crystal structure. Often those studies involve electron microscopic and electron diffraction size and structure determinations and correlations with spectroscopic properties of the growing crystallites.[2-4] Such measurements, while providing a wealth of information, are naturally limited to events occuring at relatively long times after initiation of the growth process, beyond the nucleation stage. More recently Tanaka and Iwaski applied the stopped-flow technique to study

† Permanent address: Department of Chemistry, Clarkson College of Technology, Potsdam, NY 13676.

(1) James, T. H. *The Theory of the Photographic Process*; Macmillan: New York, 1977.

(2) Klein, E.; Moisar, E. *Ber. Bunsen-Ges. Phys. Chem.* **1963**, *67*, 349, 356, 949.

(3) (a) Berry, C. R.; Skillman, D. C. *J. Appl. Phys.* **1962**, *33*, 1900. (b) *Ibid. J. Phys. Chem.* **1963**, *67*, 1827. (c) *Ibid. J. Phys. Chem.* **1964**, *68*, 1138.

(4) (a) Saijo, H.; Iwasaki, M.; Tanaka, T.; Matsubara, T. *Photogr. Sci. Eng.* **1982**, *26*, 92. (b) Tanaka, T.; Saijo, H.; Matsubara, T. *J. Photogr. Sci.* **1979**, *27*, 60.

0002-7863/88/1510-4882$01.50/0